Struct Multidisc Optim (2011) 43:165–180
DOI 10.1007/s00158-010-0563-1

RESEARCH PAPER

# Application of layout and topology optimization using pattern gradation for the conceptual design of buildings

**Lauren L. Stromberg · Alessandro Beghini · William F. Baker · Glaucio H. Paulino**

Received: 2 June 2010 / Revised: 25 July 2010 / Accepted: 25 July 2010 / Published online: 23 September 2010


**Abstract** This paper explores the use of manufacturing-type constraints, in particular pattern gradation and repetition, in the context of building layout optimization. By placing constraints on the design domain in terms of number and variable size of repeating patterns along any direction, the conceptual design for buildings is facilitated. To substantiate the potential future applications of this work, examples within the context of high-rise building design are presented. Successful development of such ideas can contribute to practical engineering solutions, especially during the building design process. Examples are given to illustrate the ideas developed both in two-dimensional and three-dimensional building configurations.

**Keywords** Topology optimization · Pattern gradation · High-rise buildings · Material layout · Pattern constraints

## 1 Introduction

The spatial arrangement of material, often known in the literature as the layout problem, is of key importance for the design and usability of many engineering products (Cagan et al. 2002). Specifically, in building design, the manner in which material is distributed is significant for engineers to develop a lateral bracing system or create a conceptual design for structural members.

While topology optimization is a very powerful tool for design, often the resulting topologies produced consist of complex geometries and poor material layouts which are of limited value to real-world problems due to expense and ease of manufacturing. An example of a typical topology optimization result without manufacturing constraints is given in Fig. 1. Therefore, in order to make the results more significant from an engineering perspective, several constraints can and should be imposed as in Fig. 1c and d with symmetry and pattern gradation constraints. For example, Guest et al. (2004) presented a method to limit the minimum member size through a fixed-length scale. This method projects the neighboring design variables onto the element density, which also alleviates numerical instabilities such as checkerboarding (patches of alternating black and white material) or mesh dependence (different solutions for different levels of mesh refinement). Similarly, Almeida et al. (2009) developed a method to control the minimum hole size by proposing an inverse projection scheme. The work by Le (2006) implements a minimum length scale to eliminate undesirable patterns in the topological design space by introducing additional layers of design variables. By adapting and applying these technologies, structural engineers can extend topology optimization to design the structural systems of buildings by looking at the constraints on the size and shape of the available materials. Moreover, the minimum member size control has been included in this work to achieve meaningful results.

Alternatively, several sensitivity and density filters have been developed as manufacturing constraints as well. Bourdin (2001) proposed a filtering technique by regularizing the density field through the use of a convolution operator to replace the point-wise element densities.

L. L. Stromberg · G. H. Paulino (✉)
Department of Civil and Environmental Engineering,
Newmark Laboratory, University of Illinois at Urbana-Champaign,
205 N. Mathews Avenue, Urbana, IL 61801, USA
e-mail: paulino@illinois.edu

A. Beghini · W. F. Baker
Skidmore, Owings & Merrill, LLP,
224 S. Michigan Avenue, Chicago, IL 60604, USA

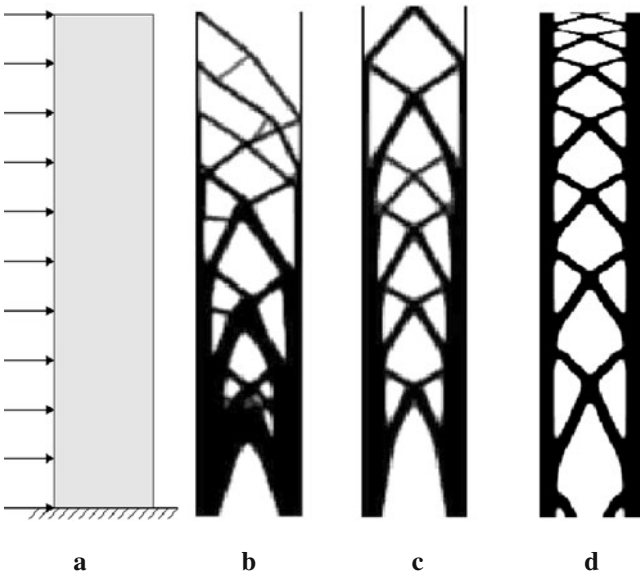


**Fig. 1** Topology optimization design for cantilever: **a** design domain subject to lateral load; **b** without consideration of manufacturing constraints; **c** with symmetry only and **d** with pattern gradation and symmetry constraints

Borrvall and Petersson (2001) also implemented a different density filter through regularized density control. Wang and Wang (2005) developed a bilateral filtering technique to perform checkerboard-free, mesh dependent, edge preserving topology optimization. Similarly, work on sensitivity filters has been done by Sigmund (1997, 2001). For a discussion on such techniques, the reader may refer to the review paper by Sigmund and Petersson (1998). Later, Sigmund (2007) proposed density filters using the idea of morphology-based black and white filters to alleviate gray regions between solid and void material, which provided control over the minimum member and hole sizes as an additional feature. An alternative to the filtering techniques is the perimeter-control studied by Ambrosio and Buttazzo (1993) and Haber et al. (1996). The use of a constraint on perimeter-control alleviated the mesh-dependence problem (in addition to the checkerboarding instability as well).

Several other geometrical manufacturing constraints have been developed for application to topology optimization, such as extrusion of a constant cross-section to produce three dimensional structures (Ishii and Aomura 2004; Zhou et al. 2002). Moreover, Zuo et al. (2006) added other constraints, including minimum hole size and symmetry to produce more practical designs by incorporating the method of moving asymptotes (MMA) with wavelets. Such techniques may be applicable and relevant for high-rise buildings.

Pattern repetition has been previously implemented in topology optimization for a variety of problems. Almeida et al. (2010) developed manufacturing constraints, specifically pattern repetition and symmetry to functionally graded materials (FGMs) on both a global and local scale. Huang and Xie (2008) used the bidirectional evolutionary structural optimization (ESO) to come up with the optimal designs of periodic structures by splitting the design domains into unit cells that are constrained to have the same material layouts. However, it has been shown that often times ESO methods can produce nonoptimal solutions (Zhou and Rozvany 2001).

Previous work has been done using periodicity, or pattern repetition, for the design of microstructures. Paulino et al. (2009) developed a material design method which combines topology optimization with homogenization to design periodic functionally graded composites. In Qiu et al. (2009), the effects of 2D periodic repetition and cyclic-symmetry for cellular structures were studied using super-elements and perimeter control. Also topology optimization has been applied to periodic microstructures in electromagnetic material for wave propagation (Nomura et al. 2009) and for lightweight cellular materials (Zhang and Sun 2006). However, rather than looking at a small scale, this work extends the application of pattern repetition to a larger scale for the conceptual design of buildings. Additionally, in modern architecture often times patterns are asymmetric to account for layout and space considerations or aesthetic value.

### 1.1 Towards efficient buildings

The next logical step is to extend the concept of pattern repetition, or periodic structures, by changing the size and shape of the patterns. In this work, this concept is described as pattern gradation. By geometrically grading such repeating patterns in a structure, or more specifically in a building, it is possible for structural engineers to come up with a conceptual design for the optimal lateral bracing systems and/or the optimal angles for the diagonal bracing to follow. Moreover, by optimizing the structural system, the consumption of resources would be reduced. According to the manual for Leadership in Energy and Environmental Design (LEED®) (LEED 2005), buildings currently account for one-third of our total energy, two-thirds of our electricity, and one-eighth of our water supply. The LEED rating system does not specifically address the problem of the minimization of the structural material use, however we consider an ethical approach to minimize the consumption of natural resources. This would significantly contribute in creating a sustainable community.

### 1.2 Practical considerations

Manufacturing constraints in topology optimization are relevant and necessary to extend the current solutions to the structural engineering industry. For instance, manufacturing constraints can be imposed on the minimum and maximum member sizes for topology optimization designs

in accordance with the available minimum and maximum sizes in the American Institute of Steel Construction (AISC) specifications for steel shapes (AISC 2005). Within these shapes, a designer must check the limit states associated with each member. Thus, a constraint on the allowable stress levels can be imposed as well.

With respect to the dynamic analysis of a structure, it may be valuable to target a certain frequency by means of a period optimization. For example, typically the first period for a building should be the longitudinal period as opposed to the torsional period since the torsional period discomforts occupants the most. Moreover, some design codes, such as the Chinese design codes (Chi 2002, 2003), enforce that the ratio of the longitudinal and torsional periods must be higher than a certain value. This situation introduces the necessity for manufacturing constraints on the periods of a structure.

In the design phase of a building, for example, one may need to run a pipe through a beam to integrate the structural system with the mechanical, electrical and plumbing systems. A manufacturing constraint on a minimum or maximum hole size in a domain could be applied in this situation to create a conceptual design for the beam which incorporates space for such a hole.

Furthermore, in regards to the glass curtain wall of a high-rise building, custom cut glass shapes typically result in very costly designs. A manufacturing constraint on the exterior cladding will decrease the need for special shapes. Here, pattern repetition is imposed so glass shapes can be cut in the same fashion and panels are repeated throughout the height of the structure.

For the structural system of a concrete building, formwork is manufactured to pour each component. With a manufacturing constraint on pattern repetition, the formwork can be reused from floor to floor, increasing the speed with which the building can be constructed. In the case of a steel building with pattern repetition, the same connections can be used throughout the height of the building. By keeping the same connections, the quality control of such connections is increased as each is repeated.

To express the need for a manufacturing constraint on the geometric pattern gradation, or the stretching and shrinking of patterns along the height of a building, we consider its structural members. Under typical loading conditions, the columns of a building will always be larger in size at its base and smaller towards the top. We introduce the pattern gradation constraint as an effective means to smoothly transition the design from one extreme to another. This concept can be further explored in the context of bracing angles. For example, due to the dominance of shear at the top of a high-rise building, the optimal bracing angle is approximately 45° (Fig. 1c). However, lower in the building there are both shear and overturning moments due to wind loads. The bracing angles near the base become like a ''high-waisted'' x-brace, with diagonals that are flatter than 45° below the intersection. A similar geometry can be noted in the principal stress trajectories described in Section 4 and Fig. 12a.

### 1.3 Paper scope and organization

Finally, we motivate this work to aid the conceptual design process of a structure by introducing manufacturing constraints in the context of layout optimization, with an emphasis placed on the pattern gradation constraint as an application for high-rise buildings. The remainder of this paper is organized as follows: in the next section, we outline the problem formulation and implementation. In Section 3, the concept of ''pattern gradation'' is introduced in the context of high-rise buildings. Then in Section 4, we discuss the mechanics of high-rise buildings and corresponding principal stress trajectories. We show numerical results for this new technique in Section 5 and conclude with a few comments on its application.

## 2 Topology optimization formulation

In this section, the topology optimization formulation is presented and the multiresolution topology optimization (MTOP) technique (Nguyen et al. 2010) is briefly reviewed and discussed in the context of this work.

### 2.1 Problem statement

Topology optimization consists of searching for the optimal layout of material in a given design domain in terms of an objective function. Throughout this work, the aim is to maximize the stiffness of the structure (i.e. building in most of the examples presented). The minimum compliance problem can be stated in terms of the density, $\rho$, and the displacements, $\mathbf{u}$, stated as follows:

$$\begin{aligned} \min_{\rho,\mathbf{u}} \quad & c(\rho,\mathbf{u}) \\ s.t. \quad & \mathbf{K}(\rho)\mathbf{u} = \mathbf{f} \\ & \int_{\Omega} \rho \, dV \leq V_s \\ & \rho(\mathbf{x}) \in [0,1] \, \forall \, \mathbf{x} \in \Omega \end{aligned} \tag{1}$$

The compliance of the structure is denoted by $c$, $\mathbf{K}(\rho)$ represents the global stiffness matrix which depends on the material densities, while $\mathbf{u}$ and $\mathbf{f}$ are the vectors of nodal displacements and forces, respectively. The volume constraint, $V_s$, represents the maximum volume permitted for the design of the structure. The design, or topology of the solution, is determined by the material density, $\rho$: a zero density value signifies a void whereas one represents solid material.

It is well-known that the topology optimization problem presented here is ill-posed, or lacks a solution in the continuum setting (Peterson and Sigmund 1998; Kohn and Strang 1986a, b, c). Thus, by applying relaxation to allow continuous variation of density in the range $[\rho_{\min}, 1]$, rather than restricting each density to an integer value of 0 or 1, the existence of a solution is guaranteed. Here, $\rho_{\min}$ is a small parameter greater than zero specified to avoid singularities of the global stiffness matrix, $\mathbf{K}(\rho)$.

For example, the Solid Isotropic Material with Penalization (SIMP) (Rovzany et al. 1992; Zhou and Rovzany 1991; Bendsoe 1989; Bendsoe and Sigmund 1999) model expresses the stiffness for each element as a function of the density using the following well-known power-law relationship:

$$\mathbf{E}(\mathbf{x}) = \rho(\mathbf{x})^p E^0 \tag{2}$$

where $E^0$ describes the Young's modulus of the solid material and $p$ is a penalization parameter with $p \geq 1$. Here, the material properties are continuously dependent on the amount of material at each point. By penalizing the densities, the stiffness for any $\rho < 1$ is small compared to its contribution toward the volume, leading the density towards 0 or 1 rather than remaining in the intermediate range. Moreover, the overall optimization is influenced towards the desired solid-void design and the discrete nature of the design can be recovered.

### 2.2 Multiresolution topology optimization implementation

The work presented here extends the multiresolution topology optimization (MTOP) scheme by Nguyen et al. (2010) to buildings, where each finite element of the displacement mesh contains several density elements. This implementation allows high-resolution designs without increasing the computational cost. In MTOP, three distinct meshes are superimposed: the displacement mesh for the finite element analysis, the density mesh to represent the material distribution over the domain, and the design variable mesh to perform the optimization (see Fig. 2). The design variable mesh is distinct from the density mesh since the density of each element is computed using a projection scheme (see Guest et al. 2004; Almeida et al. 2009) by projecting a region of design variables onto each element density. Then, the resulting element densities are used in the computation of the element stiffness matrices and sensitivities.

Some issues arise concerning the integration of the stiffness matrix. Since MTOP elements are used in this work, a study was conducted to determine whether or not the results would benefit from using a higher-order of integration. Notice that each element contains several density elements which are used to compute the element stiffness matrix. For an MTOP element with 25 design variables and densities per displacement element, denoted as Q4/n25, quadrature orders varying from 2 to 5 were investigated. The optimization of a half-MBB beam was carried out as shown in Fig. 3 with varied Gauss quadrature rules for the same resolution meshes. The compliance values are given for the respective rules. Here, the FEA is performed on a mesh of $60 \times 20$ elements with a $240 \times 80$ design variable mesh, or 16 design variables and densities per Q4 displacement element (MTOP Q4/n16 elements) as shown in Fig. 3b. The results presented confirm that $2 \times 2$ Gaussian integration is satisfactory, since the computed sensitivities and objective functions are essentially the same (see Table 1).

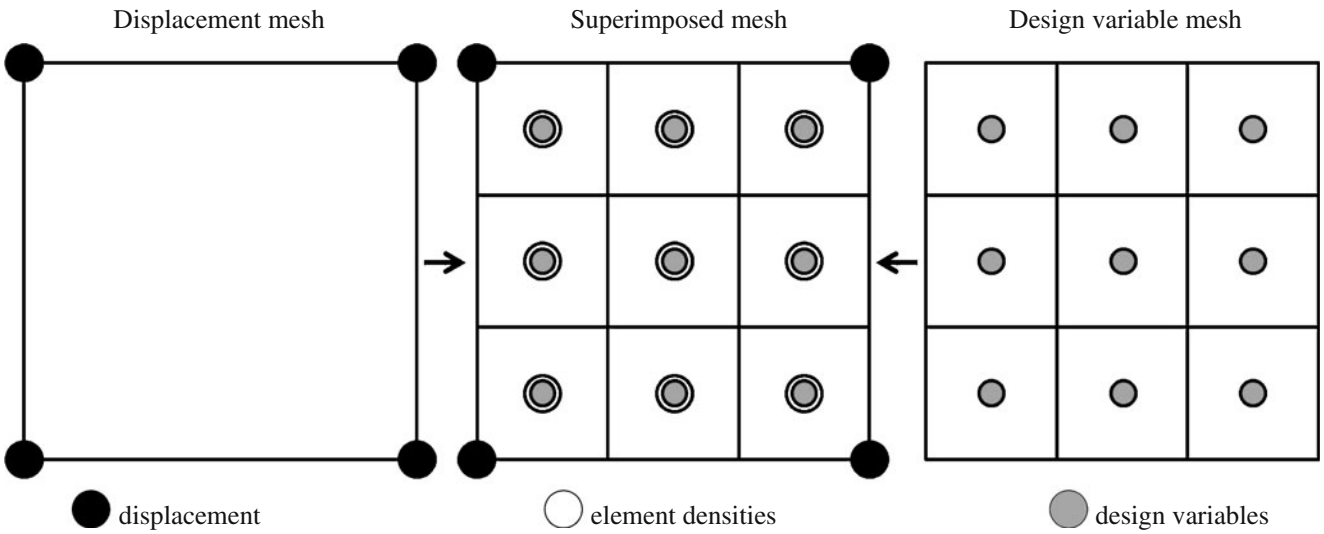


**Fig. 2** Sample MTOP meshes for Q4/n9 element

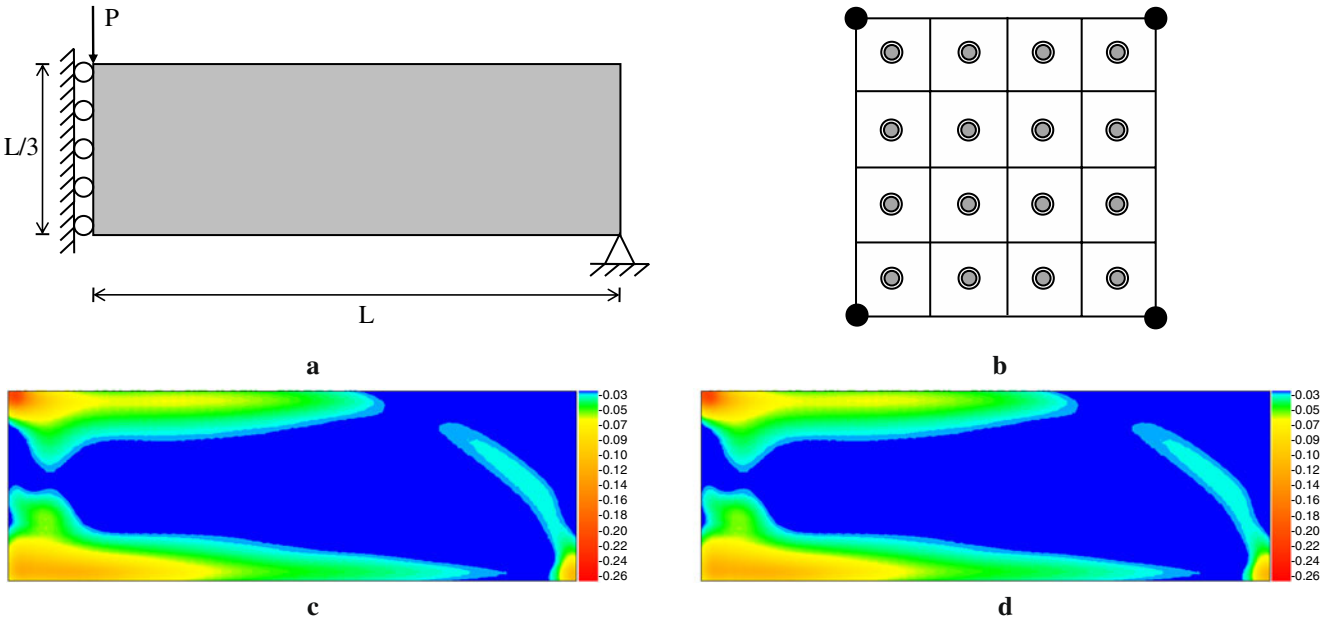


**Fig. 3** Comparison of sensitivities considering 60 × 20 element densities with 240 × 80 design variables: **a** MBB beam; **b** Q4/n16 element; **c** results with Gauss quadrature of order 2; **d** results with Gauss quadrature of order 5

To validate the MTOP approach for this work, the effect of varying the levels of refinement of the FEM mesh verses the design variable mesh were studied for a constant order of Gauss quadrature. The results are presented in Table 2. As expected, as the finite element mesh is refined for a constant design variable mesh, monotonic convergence is observed. Moreover, this sensitivity analysis shows similar results for a refinement level of 16 design variables per finite element as three finite elements per design variable (Fig. 4).

**Table 1** Values of compliance for different orders of integration considering CAMD MTOP elements

| Element density mesh | Quadrature order | Compliance |
|---|---|---|
| 30 × 10 | 2 | 209.9 |
| | 3 | 209.9 |
| | 4 | 209.9 |
| | 5 | 209.9 |
| 48 × 16 | 2 | 210.7 |
| | 3 | 210.7 |
| | 4 | 210.7 |
| | 5 | 210.7 |
| 60 × 20 | 2 | 211.3 |
| | 3 | 211.3 |
| | 4 | 211.3 |
| | 5 | 211.3 |
| 120 × 40 | 2 | 213.5 |
| | 3 | 213.5 |
| | 4 | 213.5 |
| | 5 | 213.5 |
| 240 × 80 | 2 | 215.8 |
| | 3 | 215.8 |
| | 4 | 215.8 |
| | 5 | 215.8 |

## 3 Pattern gradation

The concept of pattern gradation is introduced as a new constraint in the context of layout optimization. In this work, a ‘‘pattern’’ is defined as the number of times a particular geometric feature repeats over a domain (see Stromberg et al. 2009). Here, the ideas behind pattern repetition constraints in topology optimization designs (sometimes known as ‘‘periodic structures’’) are discussed with an application to

**Table 2** Values of compliance for different levels of refinement of FEM meshes for CAMD MTOP elements

| Design variable | Element density | Compliance |
|---|---|---|
| 240 × 80 | 30 × 10 | 209.9 |
| | 48 × 16 | 210.7 |
| | 60 × 20 | 211.3 |
| | 120 × 40 | 213.5 |
| | 240 × 80 | 215.8 |
| | 480 × 160 | 218.2 |
| | 720 × 240 | 219.6 |
| | 960 × 320 | 220.6 |

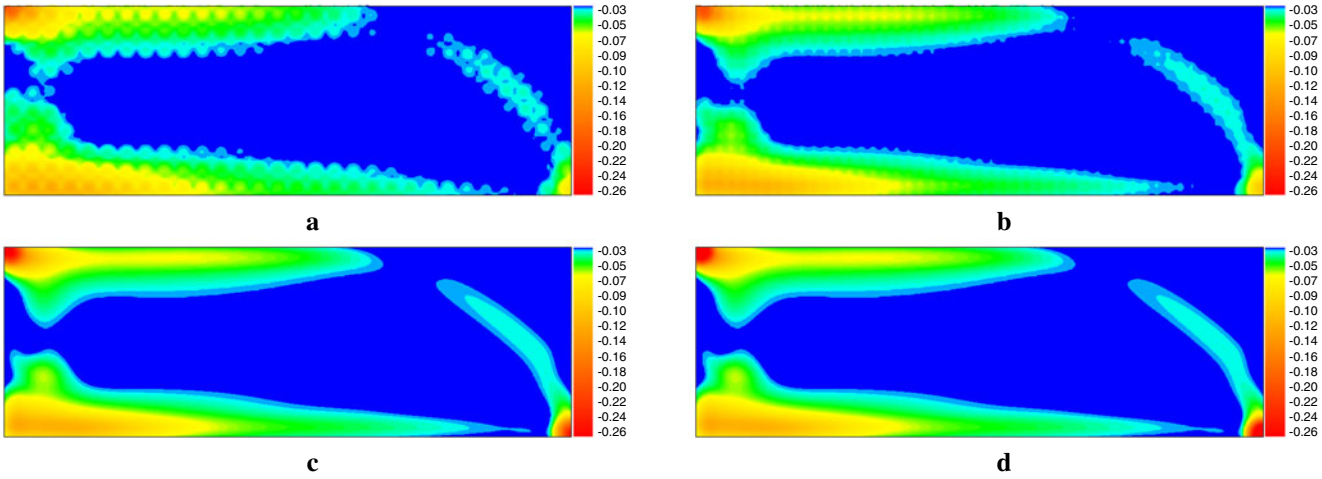


**Fig. 4** Study of the influence of various finite element meshes on the sensitivities for a constant design variable mesh of size 240 × 80: **a** 30 × 10; **b** 48 × 16; **c** 240 × 80; **d** 960 × 320

the geometric stretching and shrinking of these patterns over the domain (referred to as gradation). Furthermore, a mapping scheme is proposed to map design variables from one pattern to the next throughout the domain for the element-based and continuous approximation of material distribution (CAMD) approaches as presented in Section 2. Following, the advantages and disadvantages of each technique are briefly discussed.

The key idea behind the pattern gradation for the conceptual design of buildings presented in this work is a mapping scheme between design variables. The mapping scheme proposed in this section allows patterns of different sizes to be repeated along the height of a building to satisfy the constraints for shear and overturning moments. To achieve such constraints for any set of graded patterns, the largest pattern is considered first. The design variables from the mesh over the domain that the largest pattern covers are projected onto the smaller domains using two different techniques—one for the element-based approach and another for the CAMD. These approaches are discussed below.

## 3.1 Element-based mapping scheme

To incorporate the pattern gradation constraint, the topology optimization problem statement must be revised to incorporate this additional constraint. The new problem statement in terms of the design variables, $\rho_d$ and nodal displacements, $\mathbf{u}$ is

$$\begin{aligned} \min_{\rho_d,\mathbf{u}} \quad & c\big(\rho_d,\mathbf{u}\big) \\ s.t. \quad & \mathbf{K}\big(\rho_d\big)\mathbf{u}=\mathbf{f} \\ & \int_\Omega \rho\big(\rho_d\big)\,dV \le V_s \\ & \rho(x)\in[0,1]\,\forall\, x\in\Omega \end{aligned} \tag{3}$$

where the element densities and the design variables now become independent. Thus, the compliance and stiffness can be expressed in terms of the design variables $\rho_d$. The element densities $\rho_e$ are a function of the design variables through a mapping scheme.

### 3.1.1 *Gradation along one axis*

For the element-based approach mapping in one direction, the largest domain is first saturated with design variables at the element nodes. These design variables are considered as the primary design variables (shown in gray in Fig. 5). The primary design variables are mapped onto the smaller domains to create the mapped design variables (shown in black in Fig. 5). Here, each pattern domain is shown by the gradient colored pattern. Then, the element densities are computed using projection over the entire domain of design variables, which include both the primary and mapped design variables.

For gradation in one direction, a pattern is defined by the region of the design domain partitioned by two coordinates, denoted $x_{n-1}$ and $x_n$, respectively, for the $n$th pattern. In

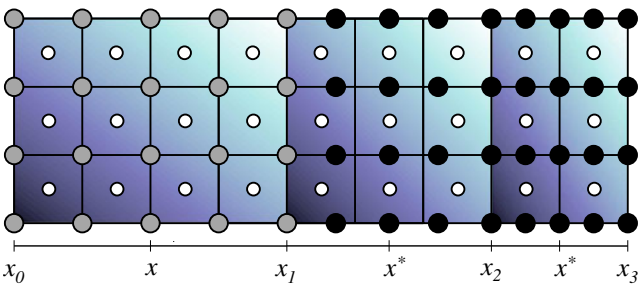


**Fig. 5** Illustration of element-based mapping scheme from $x$ to $x^*$ for pattern gradation along one axis. Mapped design variables are shown in *black* and three pattern constraints are highlighted in *gradient color*

Fig. 5, for example, the pattern gradation is being performed in the x-direction. Thus, we specify pattern 1 by selecting the coordinates $x_0$ and $x_1$ as bounds. This concept is carried over for each of the $n$ patterns.

The proposed mapping scheme for gradation in the x-direction gives the locations of the mapped design variables, $x^*$ with respect to the pattern sizes as

$$x^* = \sum_{i=0}^{n-1} (x_{i+1} - x_i) + \alpha_n (x - x_n) \tag{4}$$

where $\alpha_n$ is a scaling factor of the $n$th pattern from the largest domain (which holds the primary design variables). This scaling parameter $\alpha_n$ is defined as:

$$\alpha_n = \frac{x_{n+1} - x_n}{x_1 - x_0} \tag{5}$$

Similarly, for one directional gradation along the y-axis:

$$y^* = \sum_{i=0}^{n-1} (y_{i+1} - y_i) + \beta_n (y - y_n) \tag{6}$$

where $y^*$ is the location of the mapped design variable and $y$ is the location of the original design variable. Correspondingly, the scale factor is:

$$\beta_n = \frac{y_{n+1} - y_n}{y_1 - y_0} \tag{7}$$

For the element-based approach, the values of mapped design variables correspond to the values of the primary design variables, $\rho^* = \rho$; only the locations of these points change during the mapping scheme. The optimization on the design variables of the largest section is performed first and the subsequently smaller sections are updated. More details on the computational implementation are included in the following section.

### 3.1.2 Gradation along two or three axes

The mapping scheme can be extended for gradation in two directions following a two step procedure: the patterns are graded along one axis first using the largest pattern. Subsequently, these patterns are graded in the other direction using the patterns from the initial gradation. For example, if the patterns are graded along both the x and y axes, first the largest pattern is selected. This pattern is mapped along the x axis using the gradation scheme. Later, these patterns are mapped along the y axis. A schematic of this mapping procedure is shown in Fig. 6. For the bidirectional gradation, (4) and (6) still apply, but they are performed sequentially.

Furthermore, this technique can be generalized to three dimensions by the same procedure. For example, for pattern gradation along the x, y, and z axes the largest pattern

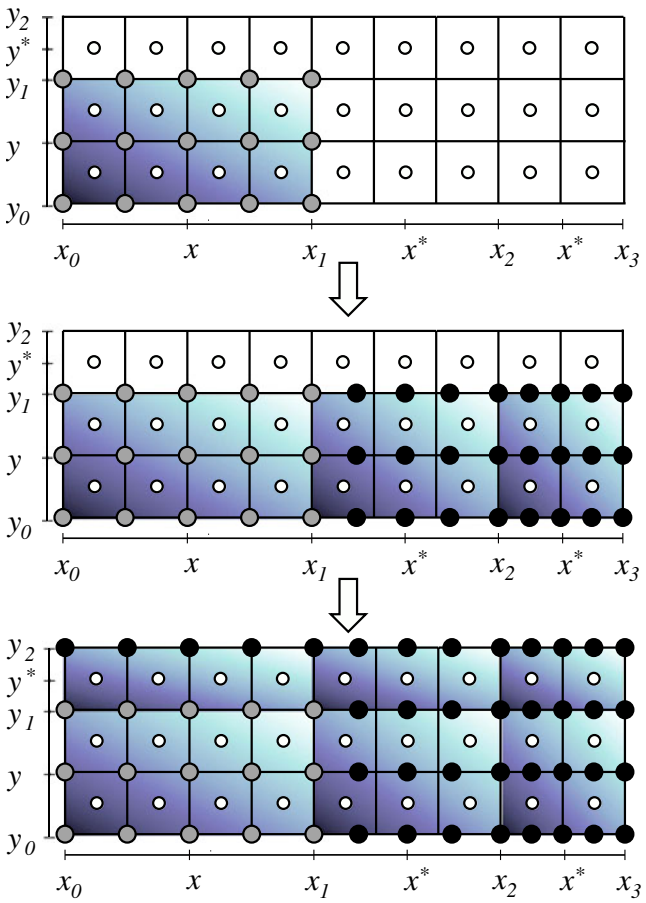


**Fig. 6** Schematic for gradation in two directions. Mapped design variables are shown in *black*

is mapped sequentially in these three directions. Equation (4) could be generalized to a third direction by replacing $\alpha_n$ with some other scale factor, $\gamma_n$, and $(x^* - x_d^*)$ with $(z^* - z_d^*)$ as follows:

$$z^* = \sum_{i=0}^{n-1} (z_{i+1} - z_i) + \gamma_n (z - z_n) \tag{8}$$

where

$$\gamma_n = \frac{z_{n+1} - z_n}{z_1 - z_0} \tag{9}$$

## 3.2 Continuous approximation of material distribution mapping scheme

The CAMD method considers a continuous material field over the design domain. Therefore, it is necessary to compute the densities for the mapped domains at the nodes to accurately approximate this material field. The following interpolation method is proposed to compute the nodal densities for each of the $n$ mapped patterns. The nodes of

the largest pattern are first mapped onto the domains of the smaller patterns similar to the element-based scheme described by (4) and (6). The densities at the nodes of the smaller patterns are then computed by interpolating the mapped nodal densities of the largest pattern. The notation $\rho_d^*$ and $\rho_{d+1}^*$ is introduced for the mapped nodes closest to any node of the $n$ patterns (see Fig. 7). The equation for the mapped densities is

$$\rho^* = \rho_d + \frac{x^* - x_d^*}{\alpha_n}\left(\rho_{d+1} - \rho_d\right) \tag{10}$$

where $x_d^*$ marks the location of the mapped design variable $\rho_d$ in the current $n$th pattern, $\rho^*$ is the new mapped density calculated at $x^*$ and $\rho_d$, $\rho_{d+1}$ are the nodes of the largest design domain to interpolate from (Fig. 7), and $\alpha_n$ is still described by (5). If $\alpha_n$ is replaced with $\beta_n$ or $\gamma_n$ and $(x^* - x_d^*)$ with $(y^* - y_d^*)$ or $(z^* - z_d^*)$ the gradation would be performed in the y-direction or z-direction instead of the x-direction. Additionally, the gradation in two or three directions can be carried out using the same technique described in the previous section where the largest pattern is graded in one direction first and later this set of patterns is graded in the other direction via (10). The sensitivities of the design variables need to be modified to account for the interpolation employed to compute the mapped nodal densities (see (10)). This will be described in detail later.

### 3.3 Comparison of mapping schemes

The pattern gradation described in the previous sections introduces additional computational expenses for the mapping scheme and sensitivity computations. However, these costs can be reduced by gathering the required data, such as the mapping information from the primary set of design variables to the mapped set of design variables for these schemes once, before the actual optimization is performed. For example, in the element-based approach at the beginning of the code the set of nodes in $S_d$ for each of the design variables and the mapped locations of these design variables for each of the patterns are stored to easily compute the one-to-one density mapping and chain rule for the sensitivity evaluation on the fly. Likewise, in the CAMD approach for each node the information of which densities to interpolate from is stored to compute the nodal densities in a timely fashion. Then the evaluation using the updated design variables after each iteration is straightforward since only the design variables of the largest pattern need to be optimized at each iteration.

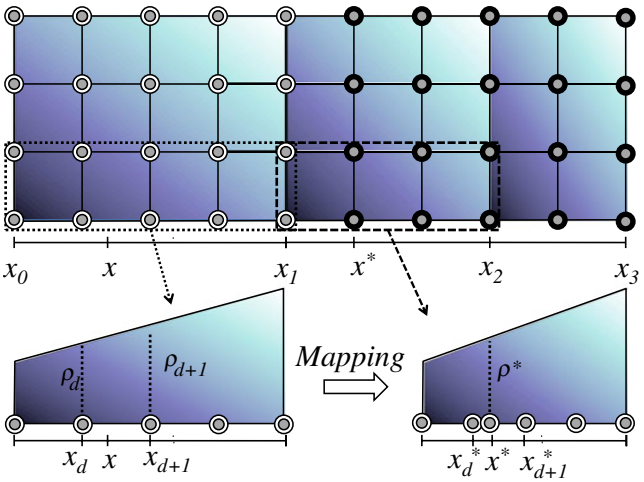


**Fig. 7** Illustration of CAMD mapping scheme: original element shown on *left*, interpolated design variables shown in *black* on *right*

The element-based mapping scheme is easier to implement but requires storing many more design variables, especially when the ratio of the size of the largest domain to the smallest one is significantly high since there will be many design variables compacted into a very small region. On the contrary, CAMD is computationally less intensive due to the smaller number of design variables. However, at the beginning of the analysis an expensive search must be performed once to find the correct primary design variables for the mapped design variables to interpolate from. Moreover, this interpolation scheme associated with the CAMD approach is by nature more expensive than the one-to-one mapping used in the element-based approach. In conclusion, the CAMD approach, despite requiring storage of a small number of design variables, is more computationally expensive.

### 3.4 Sensitivities update

The sensitivities of the design variables are computed using a chain rule since the smaller domains get their designs from the larger domains because each element density $\rho_e$ is a function of the design variables $\rho_d$ through the mapping schemes. Therefore, for both the element-based and CAMD approaches, the sensitivity of the objective function is now modified to include the chain rule as follows:

$$\frac{\partial c}{\partial \rho_d} = \sum \frac{\partial c}{\partial \rho_e}\frac{\partial \rho_e}{\partial \rho_d} \tag{11}$$

The contributions of each design variable towards the sensitivities of the primary design variables, $\rho_d$, are summed over each node of each element over the entire domain.

For the element-based scheme due to the one-to-one mapping, the sensitivity of each element density with respect to its primary design variable is

$$\frac{\partial \rho_e}{\partial \rho_d} = 1 \tag{12}$$

where $e$ is an element that gets its density from the mapping design variable $d$. Equation (11) can now be simplified as

$$\frac{\partial c}{\partial \rho_d} = \sum_{e \in S_d} \frac{\partial c}{\partial \rho_e} \tag{13}$$

where $S_d$ denotes the subset of design variables sharing the same density. For example, if there are $n$ patterns present, $S_d$ contains $n$ values.

In the CAMD mapping scheme, the sensitivities of each node must include the contributions from the nodes that are interpolated from $\rho_d$ and $\rho_{d+1}$. Thus, for each mapped element $e$ the following two relationships ensue:

$$\frac{\partial \rho_e}{\partial \rho_d} = 1 - \frac{x^* - x_d^*}{\alpha_n} \tag{14}$$

and

$$\frac{\partial \rho_e}{\partial \rho_{d+1}} = \frac{x^* - x_d^*}{\alpha_n} \tag{15}$$

In these equations $\alpha_n$ describes the gradation in the x-direction. The gradation in the y-direction or z-direction is similarly derived. For gradation along two or three axes, the sensitivities are the same, but they must be computed sequentially.

### 3.5 Projection update

For the previously discussed approaches, the design domains for each repetition of a graded pattern are scaled from the largest pattern. Thus the projection weighting function must be reformulated over the graded patterns. In this work, a new projection scheme is proposed by changing the domain of influence for element $e$ to be elliptical in shape so as to satisfy the gradation constraint. This can be attributed to the fact that the mapped distances between design variables are scaled by the factor $\alpha_n$ or $\beta_n$. The ellipse has a major axis of $2r_{\min}$ and a minor axis of $2\alpha_n r_{\min}$ corresponding to a circle scaled in one direction (see Fig. 8c). Some difficulties arise when this domain of influence lies over a boundary of the patterns. Thus, a hybrid between a circular region and an elliptical region is proposed for the projection scheme (see Fig. 8b). The weights are now computed using a linear weighting function ($q = 1$) as

$$w_j^e = \begin{cases} \left(\frac{r_{\min} - r_j^e}{r_{\min}}\right)^q & r \le r_{\min} \\ 0 & r > r_{\min} \end{cases} \tag{16}$$

where $w_j^e$ is the weight for node $j$ of element $e$, $r_j^e$ denotes the length from the element which we are computing the density to the element centroid (or node) that lies in the

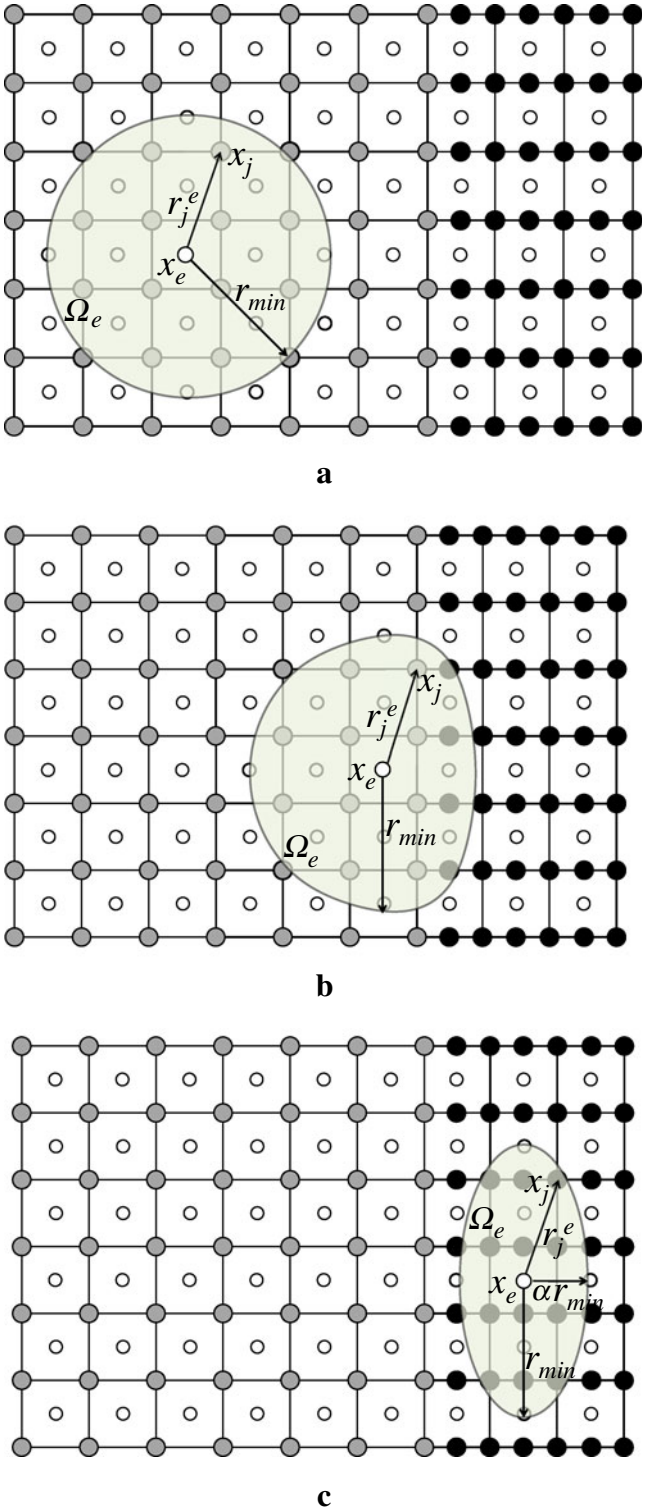


**Fig. 8** Examples of three different projection domains for pattern gradation: **a** circular; **b** hybrid and **c** elliptical. The design variables are shown in *white*; these design variables are mapped in *black* for the graded pattern

domain of influence, $\Omega_e$. Using the proposed projection, $r_j^e$ is then described by

$$r_j^e = \begin{cases} x_j - x_e & x_j \in \Omega_e,\ x_0 \le x_j \le x_1,\\ & x_0 \le x_e \le x_1 \\ \dfrac{(x_j - x_1)}{\alpha_n} + (x_1 - x_e) & x_j \in \Omega_e,\ x_1 < x_j,\ x_0 \le x_e \le x_1 \\ \dfrac{(x_e - x_1)}{\alpha_n} + (x_1 - x_j) & x_j \in \Omega_e,\ x_1 < x_e,\ x_0 \le x_j \le x_1 \\ \dfrac{(x_j - x_e)}{\alpha_n} & x_j \in \Omega_e,\ x_1 < x_j,\ x_1 < x_e \\ 0 & \text{otherwise} \end{cases} \tag{17}$$

For each element the density is then taken as the weighted average

$$\rho_e = \frac{\sum_{j\in\Omega_e} w_j^e \rho_j^e}{\sum_{j\in\Omega_e} w_j^e} \tag{18}$$

Since the element densities are computed as a function of the nodal design variables, the sensitivities must be modified as

$$\frac{\partial c}{\partial \rho_j^e} = \frac{\partial c}{\partial \rho_e}\frac{\partial \rho_e}{\partial \rho_j} = \frac{\partial c}{\partial \rho_e}\left(\frac{w_j^e}{\sum_{j\in\Omega_e} w_j^e}\right) \tag{19}$$

By using the projection method above, all of the members in the resulting design are indirectly forced to be larger than the dimension $r_{\min}$ so the optimal solutions become more reasonable to manufacture from an industrial standpoint.

These modifications allow the design to be continuous throughout the domain, while still enforcing the pattern constraints. With the revised weights above, the domain, $\Omega_e$, over which the projection is computed, remains in theory the same as a domain with no gradation in which the largest pattern is repeated $n$ times.

If a constraint on the maximum member size were of interest, the fixed length scale $r_{\max}$ (Guest 2009) could be employed by adding a constraint to specify the minimum allowed volume of voids in any particular test region. Moreover, the minimum and maximum member size constraints may be coupled by imposing both constraints for the minimum and maximum volume of voids to give designers more control over manufacturability and cost. As an alternative approach, Almeida et al. (2009) considers an inverse projection scheme to enforce a minimum hole size in the final topology. For the inverse projection, the element densities are computed using the following weights instead of those in (16) given by

$$w_j^e = \left(\frac{r_j^e}{r_{\min}}\right)^q, \quad r \le r_{\min} \tag{20}$$

Using this scheme, both the minimum hole size and the minimum member size must be of at least radius $r_{\min}$.

One more important point to consider is that for either of the direct or inverse projections presented, the weighting function does not necessarily have to be linear as shown. Alternate power-law weighting functions, such as parabolic, cubic, etc. can be generated by raising the expressions given in (16) and (20) to the power $q > 1$. Additionally, other forms of weighting functions (sinusoidal, exponential, logarithmic, etc.) for the projection scheme could be explored.

## 4 Principal stresses and high rise building mechanics

Prior to describing some numerical results based on the theory outlined in the previous sections, a few basic ideas on high-rise buildings behavior are described in this section.

The prototypical problem for the design of a high rise building is the problem of a vertical cantilever beam fixed at the top of the foundation. The fundamental laws of mechanics controlling such a problem are rather simple, being the problem statically determinate, yet very powerful. For the sake of brevity, we only underline a few fundamental properties characterizing the behavior of this structure, in particular in relation to the concept of principal stress trajectories.

The problem under consideration is described in Fig. 9 where a high-rise building of aspect ratio H/B and unitary thickness is loaded under a uniform wind load, $w$. Wind load profiles are technically represented by power laws with exponent depending on the exposure (i.e.: the building location in relation to the surroundings: urban areas, coastal regions, open country, etc.); however a uniform load distribution captures the fundamental aspects of the problem without introducing unnecessary complexity. Using simple

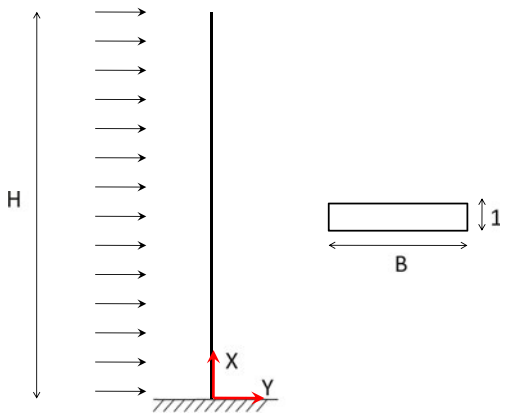


**Fig. 9** Cantilever beam of rectangular cross section

statics, the moment and shear diagram with respect to the elevation $x$ can be calculated as follows:

$$M(x) = \frac{wH^2}{2}\left(1 - \frac{x}{H}\right)^2$$
$$V(x) = wH\left(1 - \frac{x}{H}\right) \tag{21}$$

The cantilever beam problem is treated according to the Euler−Bernoulli beam theory, which hinges upon two important assumptions: the cross section stays plane during the deformation process and remains orthogonal to the beam centerline. Both these assumptions are not accurate for high-rise buildings due to the presence of shear lag and shear deformation; however, as mentioned already, the scope of this paper is to establish a theoretical benchmark against which to compare the numerical results. To this end, we deem the Euler−Bernoulli theory as providing sufficient accuracy.

The simple expressions in (21) are employed to calculate the flexural $\sigma_x$ and shear $\tau_{xy}$ stresses in the cantilever beam under consideration (see Fig. 10 for notation). Notice that in a beam the stresses $\sigma_y$ are assumed negligible. The formulas to calculate $\sigma_x$ and $\tau_{xy}$ from the centerline moment and shear according to Saint Venant's Principle for various cross sectional shapes can be found in a variety of solid mechanics textbooks (Sokolnikoff 1951; Timoshenko and Goodier 1987; Love 1944). The plane stress state described by $\sigma_x$ and $\tau_{xy}$ can be rotated in the principal coordinate system to derive the principal stress directions for the principal stresses $\sigma_1$ and $\sigma_2$ by solving the following equations derived from the Mohr's circle:

$$\tan 2\phi = \frac{2\tan\phi}{1-\tan^2\phi} = \frac{2\tau}{\sigma} = A(x, y)$$
$$\tan\phi = \frac{dy}{dx} = -\frac{1}{A} \pm \sqrt{\frac{1}{A} + 1} \tag{22}$$

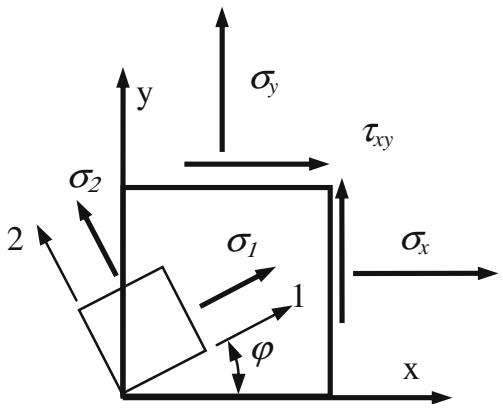


**Fig. 10** Sign convention for the stress

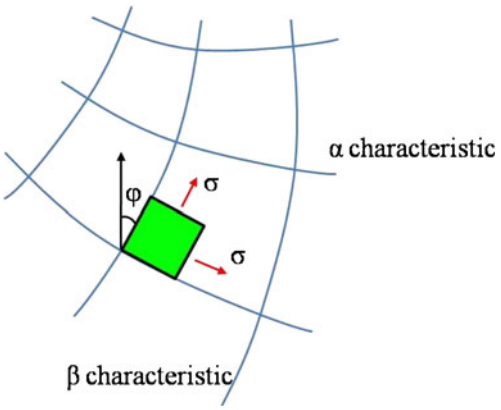


**Fig. 11** Characteristic lines obtained by solving the hyperbolic partial differential equation governing the principal stress problem

The solution of the above equations leads to two sets of characteristic lines (see Fig. 11); along these lines there is no shear stress and the normal stress is acting at each location along the tangent to the line. Equation (22) has been solved by finite difference to trace a discrete number of principal

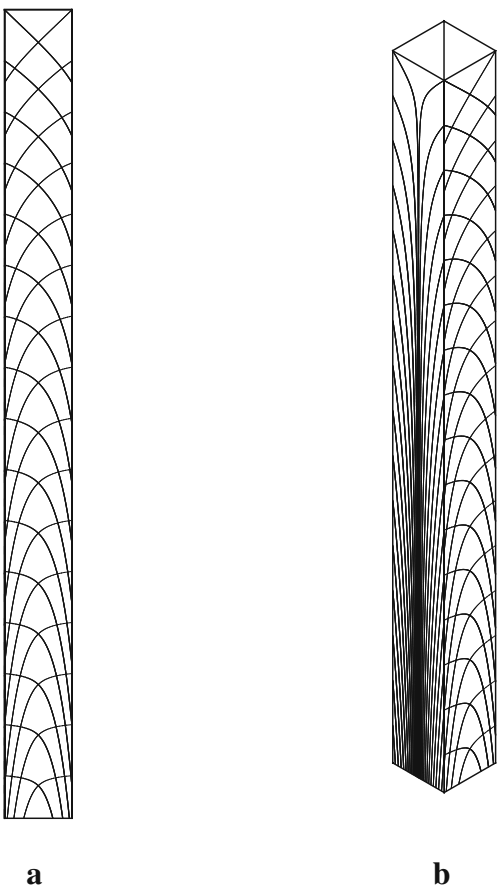


**Fig. 12** Elevation of the principal stress trajectories for the cantilever problem: **a** two-dimensional planar problem; **b** three-dimensional problem for a tubular building subject to wind loading

stress trajectories for the cantilever beam problem considered (see Fig. 12a). One set of lines represent compression lines while the other set represents tension lines. The trajectories are acting as streamlines such that the lateral wind force ''enters'' the continuum at a certain location along the height and flows through the trajectories to the foundation (this is due to the non-shear condition along these lines). Since the principal stress trajectories represent the natural flow of forces in the structure, they offer an analytical method to identify the optimal layout of structural material in a high-rise. The optimality comes from the idea of understanding how the forces are ''moving'' through the structure to the foundation and embrace this flow with the structural members.

The principal stress trajectories in Fig. 12a show the following important characteristics in relation to the behavior of high-rise buildings:

- the tension and compression lines meet at a 45° angle at the centerline—in beam theory there is a state of pure shear stress at the centerline.
- the stresses at the beam edges are vertical because the problem is purely axial. It can be noted how the lines become very dense toward the edges, emphasizing how in a high rise the most efficient way to carry the overturing moment is to put material as far away as possible from the neutral axis.
- the trajectories tend to be more vertical toward the base of the cantilever and closer to 45° bracing toward the top. This is caused by the fact that at the top there is mainly shear-type loading while the bottom of the cantilever is controlled by the overturning moment.

The principal stress analysis conducted in two dimensions can be extended to three dimensions assuming a cantilever beam with the cross section of a hollow tube (see Fig. 12b). In this case, when the wind is blowing orthogonally to one of the tube faces, the side of the tube parallel to the wind directions are behaving similarly to the two dimensional problem while, in the sides orthogonal to the wind direction, the stress trajectories are mainly vertical. This result emphasizes the typical behavior of a tubular high rise structure which behaves similarly to a simple I-beam section. The faces of the tube orthogonal to the wind direction are acting as flanges and mainly carry the overturning moment, while the faces of the tube along the wind direction are carrying the shear force.

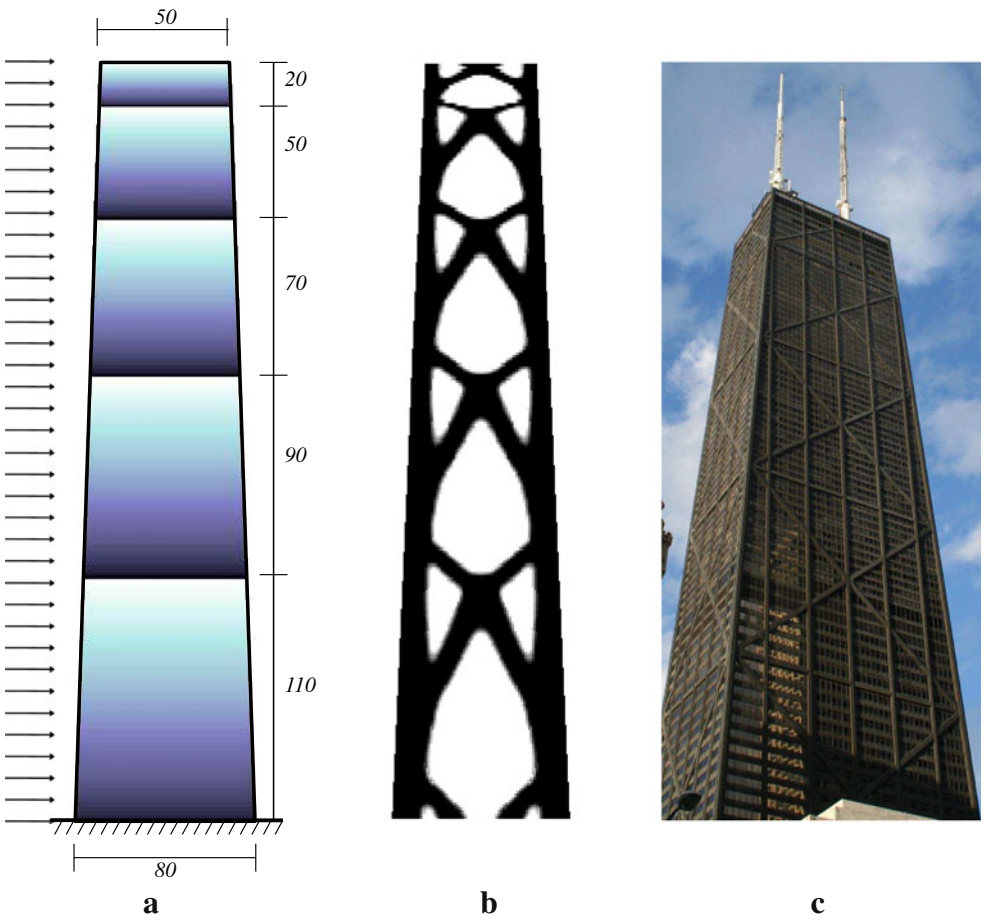


**Fig. 13** Illustration of the concept of pattern gradation along the height of a building: **a** pattern gradation constraints; **b** topology optimization result with similarities to **c** John Hancock Center in Chicago, IL (taken from en.wikipedia.org/wiki/John_Hancock_Center)

It should be noted that the analysis presented in this section is based on uniform material distribution. As the material is redistributed the paths may change.

## 5 Numerical results

The focus of this work is on the applicability of pattern repetition and layout optimization for the conceptual design of the lateral system of high rise buildings. This section focuses on a series of examples in two and three dimensions, illustrating how the methodology proposed has been used to analyze existing and conceptual structures. All examples are run using SIMP with continuation from $p = 1$ to 4 and steps of size 0.5. The Poisson's ratio is 0.3 and Young's Modulus $E = 1.0$. Examples are given next for both the element-based and CAMD approaches.

### 5.1 Domain with five patterns

The first numerical example considered is a two-dimensional tapered cantilever beam subject to wind loading and pattern constraints as displayed in Fig. 13a. The domain is $10 \times 30$ units with the fine mesh containing $80 \times 240$ elements. The volume fraction for this example is 0.5 and the minimum member size is 1.2 units. As shown in the figure, some similarities can be observed in comparison with the lateral bracing system of the John Hancock Center in Chicago, IL. In relation to the fundamental characteristics of high-rise building behavior described in the previous section, it can be noted how the material localizes at the edges to form ''columns'' and how the bracing angles change from a steeper angle at the base to a 45° angle toward the top.

### 5.2 3D tapered building under wind loading

Figures 14 and 15 illustrate the conceptual design for a diagrid structure with a square base transitioning to a circle at the top. The study is based on the SOM design of the Lotte Tower in Seoul, Korea (Fig. 14a). The meshing of this structure is illustrated in Fig. 14 where the cross-sectional views are shown along the height of the tower at

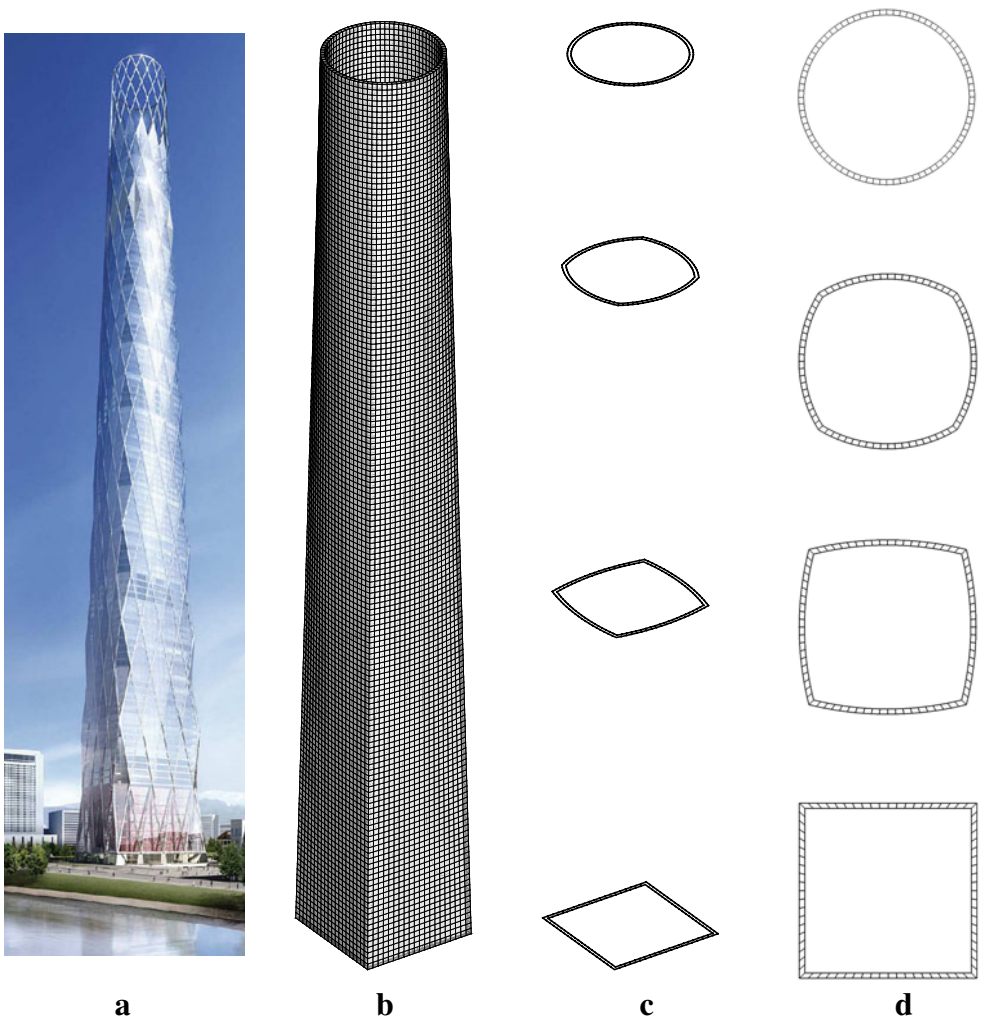


**Fig. 14** Illustration of meshing for diagrid structure: **a** SOM's Lotte Tower; **b** finite element mesh; **c**, **d** cross-section views at 0, 30, 60, and 80 m. Image **a** courtesy of Skidmore, Owings & Merrill, LLP (SOM)

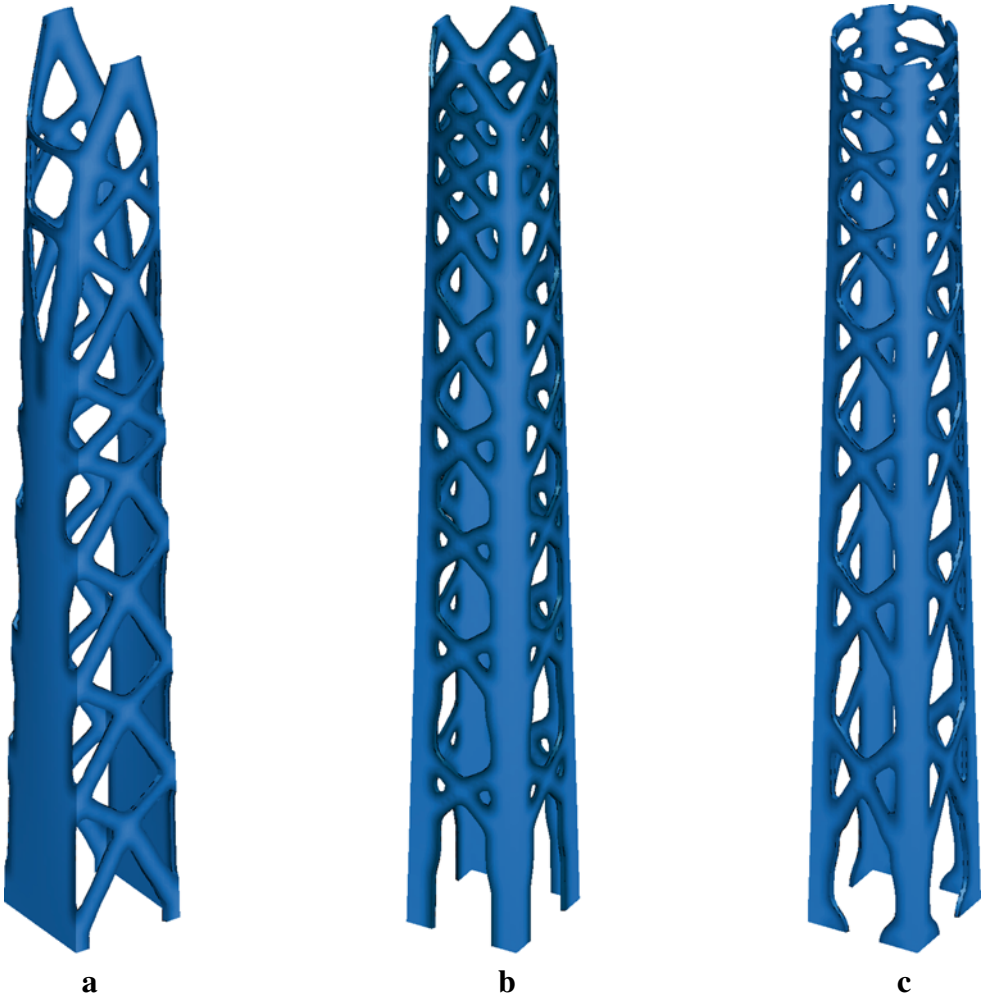


**Fig. 15** Illustration of pattern gradation for conceptual design of diagrid structure: **a** wind loading about one axis and symmetry; **b** wind loading about two axes and symmetry; **c** pattern gradation constraints

0, 30, 60, and 80 m. In Fig. 15a the results are shown for an analysis performed for wind loading in one direction without any symmetry constraint and likewise for the case with symmetry applied about two major axes in Fig. 15b.

Figure 15c shows the analysis performed with pattern gradation constraints. The design domain is $10 \times 10 \times 80$ here with a minimum member size of 1.0. The resulting designs in Fig. 15 follow the principal stress trajectories illustrated in Fig. 12 and show how the load flows in a naturally cascading pattern. In addition, the fundamental aspects of high-rise building behavior are evident: the columns increase in size from the top of the building to the base and the diagonals show larger angles of the braces at the base than at the top. Figure 15a is particularly interesting because it shows the flange-web behavior mentioned in the previous section. If no symmetry constraints are imposed, the material tends to concentrate at the structure's extreme locations, forming virtual ''flanges'' to counteract the overturning moment, while the diagonal braces counteract the shear deformation, acting like a ''web'' of an I beam.

A potential extension of this work includes the use of a more advanced data structure (see Celes et al. 2005) since it can be quite complex to use the multiresolution scheme (MTOP) for general meshes. Currently, the connectivity relationships between the coarse mesh of displacements and the fine meshes of design variables or densities are unknown. A more elaborate scheme using multiple meshes should be considered to advance this work further for general meshes.

## 6 Concluding remarks

Pattern gradation is necessary to advance topology optimization towards more practical designs for constructibility of high-rise buildings. By adding constraints on the patterns, both engineers and architects are able to develop aesthetically appealing modern designs while satisfying structural requirements. Moreover, using the techniques presented in this work, structural engineers can design the diagrid-type lateral bracing systems of buildings by identifying along the

height of the building the optimal angles for the diagonal members, therefore allowing a smooth transition between the sharp angle at the base to resist overturning moments and the shallow angle at the top to account for shear loads.

The primary contributions of this work can be briefly summarized as follows:

- Conceptual design for buildings by placing constraints on the design domain in terms of number and size of repeating patterns along any direction
- Development of mappings to geometrically grade the patterns
- Incorporation of projection techniques in conjunction with the mappings, including use of elliptical, rather than circular, domains of influence and combined shapes along intersection of domains

We remark that the present exploratory work was conducted using a continuous topology optimization formulation with compliance as the objective function and constraints on the pattern geometry. However, in terms of high-rise building design, objective functions other than compliance are of interest. For instance, other relevant objective functions may include deflection, stability considerations, and/or period optimization. In addition, multi-objective optimization (Carbonari and Paulino 2009), with natural frequencies as a second objective, are also of interest. In the case of nonlinear behavior, e.g. consideration of P-delta and second order effects, it may be interesting to investigate how the nonlinearity changes the original geometry that, in turn, can change the propensity of the current configuration of the structure to buckle. These, and other related topics, are currently under investigation by the authors.

**Acknowledgement** The first author gratefully acknowledges the support from the National Science Foundation Graduate Research Fellowship Program (GRFP).

## Nomenclature

| | |
|---|---|
| $c$ | compliance of the design |
| $E^0$ | Young's Modulus of solid material |
| $\mathbf{f}$ | global load vector |
| $\mathbf{K}$ | global stiffness matrix |
| $m$ | number of nodes of the finite element |
| $n$ | number of patterns in one direction (x, y, or z) |
| $p$ | penalization factor for SIMP |
| $q$ | degree of projection weighting function |
| $r_j^e$ | radius from centroid of element $e$ to node $j$ |
| $r_{\min}$ | minimum radius of projection |
| $r_{\max}$ | maximum radius of projection |
| $\mathbf{u}$ | global displacement vector |
| $V_s$ | maximum volume constraint |
| $w_j^e$ | projection weight of node $j$ of element $e$ |
| $\mathbf{x}$ | location of a point in the domain |
| $x^*$ | point inside a mapped pattern |
| $x_n$ | minimum bound of pattern $n$ in x-direction |
| $x_{n+1}$ | maximum bound of pattern $n$ in x-direction |
| $y_n$ | minimum bound of pattern $n$ in y-direction |
| $y_{n+1}$ | maximum bound of pattern $n$ in y-direction |
| $z_n$ | minimum bound of pattern $n$ in z-direction |
| $z_{n+1}$ | maximum bound of pattern $n$ in z-direction |
| $\alpha_n$ | ratio of pattern $n$ to largest pattern of domain in x-direction |
| $\beta_n$ | ratio of pattern $n$ to largest pattern of domain in y-direction |
| $\gamma_n$ | ratio of pattern $n$ to largest pattern of domain in z-direction |
| $\nu$ | Poisson's ratio |
| $\rho$ | density |
| $\rho^*$ | mapped density |
| $\rho_d$ | design variable |
| $\rho_e$ | element density |
| $\rho_j^e$ | density at node $j$ of element $e$ |
| $\rho_{\min}$ | minimum allowable density |
| $\Omega$ | design domain |
| $\Omega_e$ | domain of element $e$ |

## References

AISC (2005) AISC steel construction manual, 13th edn. American Institute of Steel Construction, Inc

Almeida SRN, Paulino GH, Silva ECN (2009) A simple and effective inverse projection scheme for void distribution control in topology optimization. Struct Multidisc Optim 39(4):359−371

Almeida SRN, Paulino GH, Silva ECN (2010) Layout and material gradation in topology optimization of functionally graded structures: a global-local approach. Struct Multidisc Optim. doi: 10.1007/s00158-010-0514-x

Ambrosio L, Buttazzo G (1993) An optimal design problem using perimeter penalization. Calc Var Partial Differ Equ 1(1):55−69

Bendsoe MP (1989) Optimal shape design as a material distribution problem. Struct Optim 1(4):193−202

Bendsoe MP, Sigmund O (1999) Material interpolation schemes in topology optimization. Arch Appl Mech 69(9−10):635−654

Borrvall T, Petersson J (2001) Topology optimization using regularized intermediate density control. Comput Methods Appl Mech Eng 190(37−38):4911−4928

Bourdin B (2001) Filters in topology optimization. Int J Numer Methods Eng 50(9):2143−2158

Cagan J, Shimada K, Yin S (2002) A survey of computational approaches to three-dimensional layout problems. Comput Aided Des 34:597−611

Carbonari RC, Paulino GH (2009) Multi-actuated functionally graded piezoelectric micro-tools design: a multiphysics topology optimization approach. Int J Numer Methods Eng 77(3):301−336

Celes W, Paulino GH, Espinha R (2005) A compact adjacency-based topological data structure for finite element mesh representation. Int J Numer Methods Eng 64(11):1529−1556

Chi (2002) National standard of the People's Republic of China, code for design of concrete structures, GB 50010-2002. Ministry of Construction of the People's Republic of China

Chi (2003) National standard of the People's Republic of China, code for design of steel structures, GB 50017-2003. Ministry of Construction of the People's Republic of China

Guest JK (2009) Imposing maximum length scale in topology optimization. Struct Multidisc Optim 37(5):463−473

Guest JK, Prevost JH, Belytschko T (2004) Achieving minimum length scale in topology optimization using nodal design variables and projection functions. Int J Numer Methods Eng 61(2):238−254

Haber RB, Jog CS, Bendsoe MP (1996) A new approach to variable-topology shape design using a constraint on perimeter control. Struct Optim 11(1):1−12

Huang X, Xie YM (2008) Optimal design of periodic structures using evolutionary topology optimization. Struct Multidisc Optim 36(6):597−606

Ishii K, Aomura S (2004) Topology optimization for the extruded three dimension structure with constant cross section. JSME Int J 47(2):198−206

Kohn RV, Strang G (1986a) Optimal design and relaxation of variational problems, part I. Commun Pure Appl Math 39:1−25

Kohn RV, Strang G (1986b) Optimal design and relaxation of variational problems, part II. Commun Pure Appl Math 39:139−182

Kohn RV, Strang G (1986c) Optimal design and relaxation of variational problems, part III. Commun Pure Appl Math 39:353−377

Le C (2006) Achieving minimum length scale and design constraints in topology optimization: a new approach. Master's thesis, University of Illinois at Urbana-Champaign

LEED (2005) LEED® for new construction & major renovations. US Green Building Council

Love AEH (1944) A treatise on the mathematical theory of elasticity, 4th edn. Dover, New York

Nguyen T, Paulino GH, Song J, Le C (2010) A computational paradigm for multiresolution topology optimization (MTOP). Struct Multidisc Optim 41(4):525−539

Nomura T, Nishiwaki S, Sato K, Hirayama K (2009) Topology optimization for the design of period microstructures composed of electromagnetic materials. Finite Elem Anal Des 45(3): 210−226

Paulino GH, Silva ECN, Le C (2009) Optimal design of periodic functionally graded composites with prescribed propertiesn. Struct Multidisc Optim 38(5):469−489

Peterson J, Sigmund O (1998) Slope constrained topology optimization. Int J Numer Methods Eng 41(8):1417−1434

Qiu K, Zhang W, Domaszewski M, Chamoret D (2009) Topology optimization of periodic cellular solids based on a superelement method. Eng Optim 41(3):225−239

Rovzany GIN, Zhou M, Birker T (1992) Generalized shape optimization without homogenization. Struct Optim 4:250−252

Sigmund O (1997) On the design of compliant mechanisms using topology optimization. Mech Struct Mach 25(4):493−524

Sigmund O (2001) A 99 line topology optimization code written in matlab. Struct Multidisc Optim 21:120−127

Sigmund O (2007) Morphology based black and white filters for topology optimization. Struct Multidisc Optim 33(4−5):401−424

Sigmund O, Petersson J (1998) Numerical instabilities in topology optimization: a survey on procedures dealing with checkerboards, mesh-independencies and local minima. Struct Optim 16:68−75

Sokolnikoff S (1951) Mathematical theory of elasticity, 2nd edn. McGraw Hill, New York

Stromberg LL, Paulino GH, Baker WF (2009) Pattern gradation and repetition with application to high-rise building design. In: 10th US national congress on computational mechanics. Columbus, OH

Timoshenko SP, Goodier JN (1987) Theory of elasticity, 3rd edn. Elsevier, New York

Wang MY, Wang S (2005) Bilateral filtering for structural topology optimization. Int J Numer Methods Eng 63(13):1911−1938

Zhang W, Sun S (2006) Scale-related topology optimization of cellular materials and structures. Int J Numer Methods Eng 68(9):993−1011

Zhou M, Rovzany GIN (1991) The COC algorithm, part II: topological geometrical and generalized shape optimization. Comput Methods Appl Mech Eng 98(1−3):309−336

Zhou M, Rozvany GIN (2001) On the validity of ESO type methods in topology optimization. Struct Multidisc Optim 21(1):80−83

Zhou M, Fleury R, Shyy YK, Thomas H, Brennan JM (2002) Progress in topology optimization with manufacturing constraints. In: Proceedings of the 9th AIAA MDO conference AIAA-2002-4901

Zuo KT, Chen LP, Zhang YQ, Yang J (2006) Manufacturing- and machining-based topology optimization. Int J Adv Manuf Technol 27(5−6):531−536